THE ASTROPHYSICAL JOURNAL, 406:L11–L14, 1993 March 20

HIGH-RESOLUTION IMAGING OF [Fe II] 1.64 MICRONS, BRACKETT-γ, AND H_2 1–0 $S(1)$ EMISSION IN THE STARBURST GALAXY NGC 253

DUNCAN A. FORBES
Institute of Astronomy, Cambridge; and Lick Observatory, University of California, Santa Cruz, CA 95064

MARTIN J. WARD
Department of Physics, Nuclear Physics Laboratory, Keble Road, Oxford OX1 3RH, England

AND

V. ROTACIUC, M. BLIETZ, R. GENZEL, S. DRAPATZ, PAUL P. VAN DER WERF, AND A. KRABBE
Max-Planck-Institut für extraterrestrische Physik, D-8046 Garching bei München, Germany
Received 1992 May 11; accepted 1992 December 31

ABSTRACT

We present 1″ resolution imaging of the nuclear region of the starburst galaxy NGC 253 in the near-infrared lines of [Fe II] 1.64 μm, Brackett-γ, and H_2 1–0 $S(1)$, together with the adjacent continuum. The data reveal an emission region extended some 10″ northeast of the nucleus, with several embedded compact peaks or hot spots. The continuum and the three spectral lines have the same general distribution but differ in detail. The line emission from H_2 and Brγ are closely matched in the circumnuclear region. However, the H_2 emission reveals wispy structures which are more prominent to the northwest of the nucleus. We propose that the Brγ and H_2 emission lines are excited in star formation regions and that the [Fe II] emission traces the distribution of supernova remnants. The hot spots are compact ($\leq$12 pc) circumnuclear star formation regions containing a mixture of H II regions, supernova remnants, and supergiants. There is evidence that many of the supernova remnants in NGC 253 may be more luminous than their counterparts in the Galaxy. These observations constrain the stellar populations in the circumnuclear region and indicate that the radio emission is dominated by nonthermal emission processes.

Subject headings: galaxies: individual (NGC 253) — galaxies: nuclei — infrared: galaxies — supernovae: general

1. INTRODUCTION

Recently Forbes, Ward, & DePoy (1991) presented a high-resolution broad-band H (1.65 μm) image of the starburst galaxy NGC 253 which revealed three or more circumnuclear hot spots. Several possible origins for these hot spots were identified, such as giant dusty H II regions, red supergiants, or reradiation from dust in a SNR shell.

In this *Letter* we present high-resolution images of NGC 253 in the emission lines of [Fe II] 1.64 μm; Brγ, and H_2. These narrow-band images provide additional information on the excitation mechanism and the distribution of SNRs, H II regions, and molecular gas in the nuclear region. The near-infrared emission lines of [Fe II] are particularly strong cooling lines in SNRs and virtually absent from H II regions (see Oliva, Moorwood, & Danziger 1989; Greenhouse et al. 1991). These lines are excited in an extended transition region of partly to fully ionized gas. Excitation by electron collisions in the cooling recombination zone behind a fast-moving shock is favored by Greenhouse et al. (1991), whereas Graham, Wright, & Longmore (1990) advocate UV and X-ray heating from photoionization as inferred for the Crab Nebula. SNRs can therefore provide the enhanced abundance of iron (the SN blast wave liberates iron from dust grains) and the ionization conditions necessary to produce the observed [Fe II] emission. A further source of shock ionization in starburst galaxies could be the large-scale shocks associated with an outflowing "superwind" (McCarthy, Heckman, & van Breugel 1987). These shocks are thought responsible for the LINER-type spectrum seen perpendicular to the disk. Another possibility, which may also give rise to the LINER spectrum, is radiatively heated Seyfert-like narrow-line clouds. Imaging in [Fe II] should allow us to distinguish between these different sources of ionization.

Molecular hydrogen (H_2) line emission can be excited by either fluorescence (due to far-UV pumping in low-density gas) or collisions in dense gas heated by shocks, UV radiation or X-rays. Moorwood & Oliva (1990) place constraints on far-UV pumping while favoring collisional excitation via X-ray heating or shocks from SNRs. If both the [Fe II] and H_2 are excited by SNRs, we would expect them to have similar distributions. However, if the dominant mechanism of collisional excitation is either relatively slow (<50 km s^{-1}) shocks within the mass outflows of young stars or far-UV radiation heating of photodissociation regions, we would expect the H_2 to resemble the Brγ emission. The Brγ recombination line probes recent massive star formation as it is produced in the H II regions surrounding OB stars. A previous image of H_2 1–0 $S(1)$ has been presented by Wright & Joseph (1989) but with significantly poorer resolution than presented here. Our results on the spatial distribution of the [Fe II] 1.64 μm, Brγ, and H_2 emission regions are reported in this *Letter*.

2. OBSERVATIONS AND DATA REDUCTION

Our observations were made using the MPE Fabry-Perot-Array-Spectrometer (FAST; Rotaciuc et al. 1991; Krabbe et al. 1993). These observations were carried out on the 4.2 m William Herschel Telescope located on La Palma, Canary Islands in 1991 July and on the 2.2 m telescope at La Silla,

Chile in 1990 January. FAST consists of a Queensgate Fabry-Perot interferometer operating between 1.9 and 2.4 μm with a spectral resolution of $R = 950$, in series with a circular variable filter (CVF) operating from 1.4 to 2.4 μm with $R = 45$. The detector is a SBRC 62 × 58 InSb array. Observations of Brγ and H_2 were obtained using the Fabry-Perot with the CVF as an order sorter; the [Fe II] images were made using the CVF alone. Typically a single frame consists of an on-chip integration time of 100 s on the line and 100 s on the corresponding continuum on either side of the line. We used an argon lamp for wavelength calibration. On the WHT we had an image scale (for [Fe II] and H_2) of 0".50 pixel^{-1}. The optical seeing was ~1".2 FWHM, resulting in a FWHM resolution of ~0".9 at 2 μm. At La Silla, the image scale was 0".78 pixel^{-1}, and the optical seeing was ~1".5, giving a resolution at Brγ of 1".3 FWHM.

The data were reduced using the MIDAS software package. Initially, a dark frame, of the same exposure time, is subtracted from each frame. The data were then flat-fielded using a sky frame obtained from the CVF shortly after the galaxy observation and sky subtracted. It is important that a very careful continuum subtraction is carried out, particularly for the [Fe II] observations because the line-to-continuum ratio is small (a few percent) and the CVF operates at low resolution. After obtaining an image on the line, the CVF is immediately stepped to obtain the continuum on both sides of the line. Spatial registration is achieved to a fraction of a pixel by autoguiding on a nearby star. Examination of the [Fe II] "on-line" image ([Fe II] line + underlying continuum) divided by an "off-line" image (the continuum shortward of [Fe II]) reveals several peaks of enhanced [Fe II] line emission over and above the continuum emission. To obtain our final [Fe II] line image we have subtracted the average continuum (from either side of the line). The accuracy of our continuum subtraction can be estimated by comparing the two off-line continuum images. In the region of interest we find an rms dispersion of ~1% which includes the intensity difference between the two continua. A similar procedure is applied to the other narrow-band images. Several frames were aligned using the peak signal and co-added to give total on-source integration times of 600, 1600, and 800 s for the [Fe II], Brγ, and H_2, respectively. Finally, the images were flux-calibrated using standard stars observed before and after the galaxy. We also obtained a 30 s broad-band K image, using the CVF, although without standard stars. All of the images have been resampled to give an effective scale of 0".25 pixel^{-1} (1" corresponds to 12 pc at an assumed distance of 2.5 Mpc).

3. ANALYSIS

3.1. *Spatial Distribution of the Near-Infrared Emission*

In Figure 1 we show images of broad-band K (2.20 μm), [Fe II] 1.644 μm, Brackett-γ 2.166 μm, and H_2 1–0 $S(1)$ 2.121 μm. We have adopted the naming convention used by Forbes, Ward, & DePoy (1991) to indicate the location of the enhanced emission. All three lines, as well as the continuum, show a similar morphology, namely a 10" extension to the NE of the nucleus plus three or more compact hot spots in the disk of the galaxy. But there are differences when examined in detail. For the [Fe II] image, which has the lowest S/N of the four images, we show only the strongest emission (ranging from 2 to 5 σ). The [Fe II] image is dominated by three bright peaks and shows no strong emission perpendicular to the disk. Hot spot

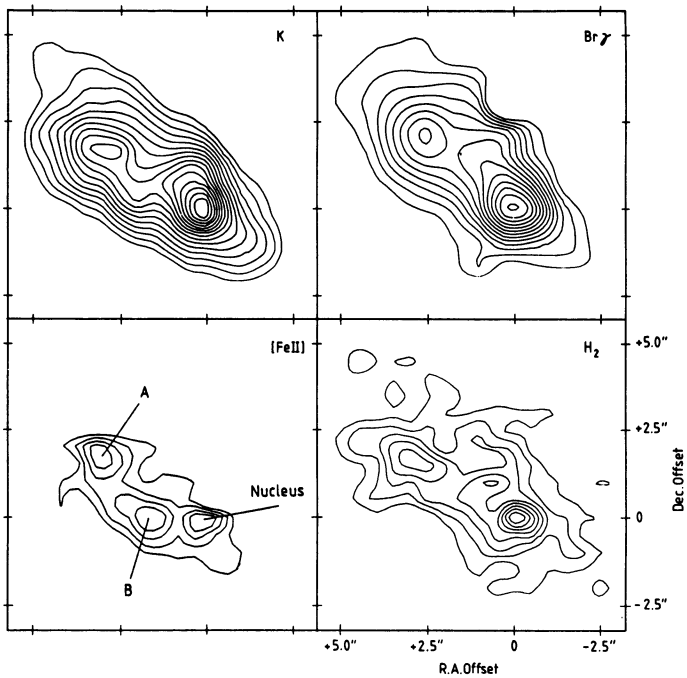

FIG. 1.—Contour maps of NGC 253 in broad-band K (2.20 μm), Brackett-γ 2.166 μm, [Fe II] 1.644 μm, and H_2 1–0 $S(1)$ 2.121 μm. The contour unit for the K map is 100 counts. For Brγ, [Fe II], and H_2 the contour units are 6.1, 35.8, and 6.5 × 10^{-17} ergs s^{-1} cm^{-2} per 0".25 pixel, respectively. The [Fe II] map indicates the location of the nucleus and hot spots A, B. North is up, and east is left in all figures.

B has no strong counterpart in the Brγ image, although the other two peaks (A and the nucleus) are clearly seen. Also present in the Brγ image is substantial emission to the north of hot spot B which appears to have no strong counterpart in the [Fe II] image. The K-band continuum image bears some resemblance to the [Fe II] image, but there are important differences, namely substantial continuum emission just north of the nucleus and location B, where the [Fe II] line emission is weak. The H_2 emission is considerably extended and reveals a remarkable similarity to Brγ in the circumnuclear region. The better sensitivity and spectral resolution in the K window reveals wispy structures in H_2 (with a S/N ~ 5–6) considerably extended to the northwest of the nucleus. Our K image, and the H image presented in Forbes et al. (1991), show a general morphological similarity to the [Fe II] image. None of the images show strong emission to the SW of the nucleus, which can be explained in terms of the increased extinction due to dust (see Scoville et al. 1985; Waller, Kleinmann, & Ricker 1988).

On the nucleus, Moorwood & Oliva (1988) measure fluxes of [Fe II] 1.64 μm, Brγ, and H_2 1–0 $S(1)$ to be 31.8, 17.9, and 11.1 respectively (in units of 10^{-14} ergs s^{-1} cm^{-2}) in a 6" × 6" entrance aperture. We find 31, 13, and 15 × 10^{-14} ergs s^{-1} cm^{-2} respectively. In Table 1 we give the narrow-band emission line flux in a 2"diameter aperture centered on the three main peaks as indicated in Figure 1.

3.2. *Radio Structure and Excitation Mechanisms*

In order to search for any spatial coincidence between the structure seen in the infrared images and the radio emission (Antonucci & Ulvestad 1988; Ulvestad & Antonucci 1991), we need to determine the absolute position of our images.

TABLE 1

EMISSION-LINE HOT SPOTS

Hot Spot	3.6 cm Radio source[a]	Brγ Flux[b]	[Fe II] 1.64 μm Flux	H_2 Flux	[Fe II]/Brγ	H_2/Brγ	Spectral Index[c]
Nucleus	5.790, 39.08	3.2	3.3	2.6	1.0	0.8	0.1
A	5.994, 37.04	2.4	5.4	2.4	2.3	1.0	−1.1
B	5.888, 38.94	1.3	7.8	2.3	6.0	1.8	...

[a] Offset in seconds of time and arcseconds from $\alpha = 0^h45^m00^s$, $\delta = -25°33'00''$ (Ulvestad & Antonucci 1991).
[b] Fluxes from a 2″ aperture measured on the emission line hot spot centroid, in units of 10^{-14} ergs s^{-1} cm^{-2}.
[c] Radio spectral index between 6 and 3.6 cm ($S \propto \nu^{\alpha}$) from Ulvestad & Antonucci 1991.

Previous astrometry (see Forbes, Ward, & DePoy 1992a) indicated that the brightest *H*-band hot spot is coincident with the radio nucleus, within their positional uncertainty. Assuming that the *H* peak lies at the same location as the radio nucleus, they found that the other compact 6 cm radio sources had a good spatial agreement with the *H*-band hot spots. We will assume that the *K* band continuum peak is also coincident with the radio nucleus, i.e., $\alpha = 0^h45^m5^s.790$, $\delta = -25°33'39''.08$ (1950).

Broad-band 12 μm imaging (Piña et al. 1992) reveals a similar structure to the near-infrared images presented here. The 12 μm emission is probably thermal reradiation from warm dust, whereas the shorter wavelength near-infrared emission has a significant contribution from supergiants. Based on their astrometry (with 1″.6 uncertainty), Pinã et al. suggest the brightest infrared peak is not associated with any strong compact radio source. We find this surprising in view of our narrow-band images which indicate that the continuum infrared peak is also the location of enhanced young star formation (as traced by Brγ), [Fe II], and H_2 emission. Clearly more accurate astrometry is required to fully resolve this matter.

Figure 2 (Plate L3) shows Brγ superposed on the [Fe II] emission (aligned using the peak signal). The lack of emission perpendicular to the disk argues strongly against shock ionization from a superwind or radiatively heated narrow-line clouds as the primary source of [Fe II] or Brγ emission. Assuming our positioning of the infrared emission peak with the radio nucleus we find that two compact 3.6 cm radio sources can be associated with hot spots A and B. These radio sources are each within 0″.25 of the hot spot centroid. The nucleus and hot spot A (labeled in Fig. 1) can be clearly seen in both [Fe II] and Brγ, suggesting that a SNR is located near or within a giant H II region. (We note that at hot spot A the [Fe II] emission is offset by about 0″.5 from the Brγ peak.) The nucleus has a flat radio spectrum suggesting a significant thermal contribution from a giant H II region, hot spot A has a somewhat steeper spectral index (see Table 1). The 3.5 cm source closest to hot spot B is weaker than at A or the nucleus and does not have an equivalent source at 6 cm; this might be due to confusion of sources at lower resolution or they could be very young SNRs (~few years). If the latter is true, the remnant would eventually become optically thin at lower frequencies resulting in a detectable 6 cm flux. We note however that the 6 cm emission from the nucleus has an extension toward hot spot B. Hot spot B has the largest [Fe II]/Brγ line ratio (6.0). This ratio, assuming no extinction, indicates the relative contributions from radiative processes associated with SNRs compared to the production of Lyman-continuum photons. For comparison, a pure star-forming region such as the Orion Nebula has a line ratio of ~0.05, whereas Galactic SNRs have values closer to 50 (Moorwood & Oliva 1988). When properly calibrated it may form a useful age diagnostic—as the SN rate remains high for $\sim 10^7$ yr after the termination of massive star formation (van der Werf et al. 1993). We note there are possible additional [Fe II] hot spots near the nucleus corresponding to locations C and D of Forbes et al. (1991), i.e., NE and SW of the nucleus, although these peaks only have a S/N ~ 2.

We also show in Figure 2 the 6 cm radio continuum superposed on the H_2 emission. The radio continuum, like Brγ, has a similar distribution to the strongest H_2 emission. This suggests that H_2 emission closely follows the distribution of star-forming regions and indicates that the excitation mechanism is directly related to young star formation. Comparison with the CO data of Canzian, Mundy, & Scoville (1988) reveals that the H_2 emission is concentrated within the densest part of the CO bar ($n \geq 10^4$ cm^{-3}). This is also the location of other molecules that trace dense gas (see Mauersberger & Henkel 1991). Submillimeter CO observations of the nucleus by Harris et al. (1991) found evidence that the molecular gas is warm ($T \geq 100$ K). The ratio of 2–1 *S*(1) to 1–0 *S*(1) in the nuclear region is 0.13 (Moorwood & Oliva 1990), which again confirms that the molecular gas is warm and dense. The H_2/Brγ line ratios, given in Table 1, are consistent with those found for a large sample of galactic nuclei (Moorwood & Oliva 1988). The dramatic wispy structure seen to northwest of the nucleus may be related to the superwind of outflowing material from the nuclear region due to multiple SN events (McCarthy et al. 1987). These SN blowout cavities in the ISM perpendicular to the disk which may give rise to the bubble-like or wispy structure seen.

If we subtract the estimated contribution from [Fe II] throughout the galaxy, then we find that the three brightest hot spots have luminosity in the [Fe II] 1.64 μm line of $\sim 10^{37}$ ergs s^{-1}. Galactic SNRs yield luminosities $\sim 10^{36}$ ergs s^{-1} (Moorwood & Oliva 1988). The [Fe II] emission is therefore enhanced if due to a single remnant. Compared to Cas A, the most luminous SNR in our Galaxy, the radio emission from the compact sources in NGC 253 is enhanced by a factor of ~5. As the [Fe II] line is sensitive to high density gas (the critical density of the $^4D_{7/2}$ state is about 2×10^5 cm^{-3}) more powerful emission may be expected in the high-density environment of a starburst nucleus. In addition, the confining medium causes the remnant to evolve more quickly, thermalizing more energy over shorter time scales. We can use the [Fe II] luminosity to estimate the number of SNs within 6″ diameter of the nucleus (i.e. roughly equivalent to the radio structure imaged by Ulvestad & Antonucci 1991). Taking the extinction-corrected luminosity to be $\sim 7 \times 10^{38}$ ergs s^{-1} (assuming $A_V = 14$, see Waller et al. 1988) gives the number of SNs required to be 70, based on the [Fe II] luminosity from an individual hot spot given above. Assuming an average age of

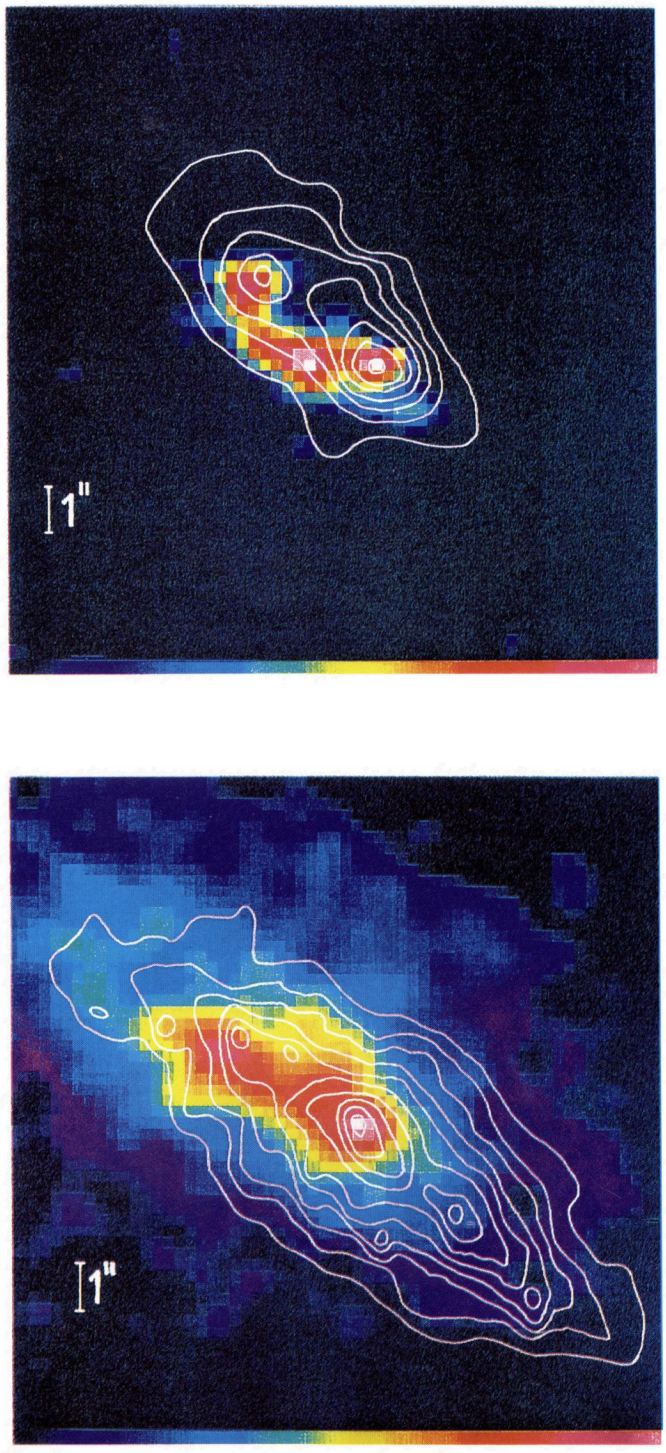

FIG. 2.—*Top*: Linear image of [Fe II] 1.64 μm, with the Brγ contour map superposed. The color features shown range from 2 to 5 σ. The contour unit is 6.1×10^{-17} ergs s^{-1} cm^{-2} per 0".25 pixel. *Bottom*: Linear image of H_2, with the 6 cm radio continuum (reproduced from Antonucci & Ulvestad 1988) superposed. The radio beam size is 0".55 × 0".31. The color features shown range from 5 to 20 σ.

400 yr for the SNRs (Antonucci & Ulvestad 1988) implies a SN rate of ~ 0.2 yr^{-1}, consistent with X-ray, radio, and far-IR estimates.

In order to estimate the number of ionizing photons (Q) available from the observed radio flux, it would be necessary to separate the thermal and nonthermal emission (which may dominate in starburst galaxies). An alternative method, that does not suffer from this problem, is to derive Q from the Brγ flux. Assuming case B recombination at 10^4 K,

$$Q = 1.0 \times 10^{51} \frac{F_{\mathrm{Br}\gamma}}{(10^{-13} \text{ ergs s}^{-1} \text{ cm}^{-2})} \frac{D^2}{(\text{Mpc})} .$$

We calculate an extinction-corrected Brγ flux of 4.7×10^{-13} ergs s^{-1} cm^{-2} in a 6″ diameter aperture. The number of ionizing photons available is therefore 2.9×10^{52} photon s^{-1}. Assuming that the average ionizing star is of type O9 (see Telesco & Harper 1980) with a flux of 1.2×10^{48} photon s^{-1} (Panagia 1973) then 2.4×10^4 such stars are required. This implies an O star formation rate of $\sim 0.1\ M_\odot$ yr^{-1} (for a $25\ M_\odot$ star with a lifetime of 5×10^6 yr) in the nucleus. Assuming a Salpeter initial mass function, the SN rate for stars above $8\ M_\odot$ is about $0.05\ M_\odot$ yr^{-1} and star formation rate for stars above one solar mass is $1.6\ M_\odot$ yr^{-1} (similar to the rate derived by Waller et al. 1988 in the central 8″).

A map of CO stellar absorption by Doyon, Joseph, & Wright (1991) indicates the presence of red supergiants (the likely progenitors of Type II supernovae) in the central 6″. Knowing the number of O stars, we can estimate the contribution to the K-band flux from supergiants. Assuming a ratio of O stars to supergiants of 5–10 (typical of Galactic OB associations; Humphreys 1978) implies 2400–4800 supergiants are present in the nuclear region. Forbes et al. (1992b) measured a K magnitude of 8.2 in a 6″ diameter aperture. After correcting for $A_V = 14$, this implies that 50%–100% of the K-band flux could be due to red supergiants (with an absolute magnitude of -11.0). A significant contribution to the K-band flux from reradiation of warm dust would favor the lower limit.

Again assuming case B recombination theory, we can deduce the thermal radio flux at 6 cm using Table 6 of Ho, Beck, & Turner (1990). Our extinction-corrected Brγ flux implies a thermal 6 cm flux of 47 mJy in the central 6″. Adding up the flux from the compact radio sources in this area (Ulvestad & Antonucci 1991) gives a total of ~ 120 mJy. Therefore most of the 6 cm radio emission in the nuclear region is nonthermal, consistent with the steep spectrum for most of the compact sources.

4. CONCLUSIONS

The narrow-band near-infrared images presented here provide useful diagnostics of the nuclear region of NGC 253. In particular, we suggest that the central 6″ of NGC 253 contain around 24,000 O stars and 3000 red supergiants along with H II regions and SNRs located throughout the nuclear region. This implies that the massive star formation rate is $\sim 0.1\ M_\odot$ yr^{-1}. We also find that more than 50% of the K-band flux is due to supergiants. The radio flux in the nuclear region is dominated by the nonthermal emission of SNRs. The H_2 emission closely follows the Brγ emission suggesting that the H_2 is excited in the mass outflows and/or dense photodissociation regions associated with young star formation. The outlying wispy structure seen in H_2 may be due to an outflowing superwind. The [Fe II] 1.64 μm emission does not appear to arise in a superwind or Seyfert-like narrow-line clouds but rather by SNRs in the disk of the galaxy. There is some evidence, from the [Fe II] and radio emission, that the SNRs in the nuclear region of NGC 253 are more luminous than their counterparts in the Galaxy. Narrow-band infrared imaging, in particular [Fe II], should be extended to a large sample of starburst and Seyfert galaxies.

We thank R. Piña, R. Puetter, A. Sternberg, and R. Terlevich for useful discussions. We also thank the observatory staff at La Silla and La Palma for their excellent support and H. Slimgerland and M. Cameron for help with the observations. Finally we thank the referee for many useful comments. D. A. F. acknowledges financial support from an Isaac Newton Studentship.

REFERENCES

Antonucci, R. R. J., & Ulvestad, J. S. 1988, ApJ, 330, L97
Canzian, B., Mundy, L. G., & Scoville, N. Z. 1988, ApJ, 333, 157
Doyon, R., Joseph, R. D., & Wright, G. S. 1991, in Astrophysics with Infrared Arrays, ed. R. Elston (ASP Conf. Ser., 14), 69
Forbes, D. A., Ward, M. J., & DePoy, D. L. 1991, ApJ, 380, L63
———. 1992a, ApJ, 385, L31
Forbes, D. A., Ward, M. J., DePoy, D. L., Boisson, C., & Smith, M. 1992b, MNRAS, 254, 509
Graham, J. R., Wright, G. S., & Longmore, A. J. 1990, ApJ, 352, 172
Greenhouse, M. A., Woodward, C. E., Thronson, H. A., Rudy, R. J., Rossano, G. S., Erwin, P., & Puetter, R. C. 1991, ApJ, 383, 164
Harris, A. I., Hills, R. E., Stutzki, J., Graf, U. U., Russell, A. P. G., & Genzel, R. 1991, ApJ, 382, L75
Ho, P. T. P., Beck, S. C., & Turner, J. L. 1990, ApJ, 349, 57
Humphreys, R. M. 1978, ApJS, 38, 309
Krabbe, A., et al. 1993, in preparation
Kronberg, P. P., Biermann, P., & Schwab, F. R. 1985, ApJ, 291, 693
Mauersberger, R., & Henkel, C. 1991, A&A, 245, 457
McCarthy, P. J., Heckman, T. M., & van Breugel, W. 1987, AJ, 93, 264
Moorwood, A. F. M., & Oliva, E. 1988, A&A, 203, 278
———. 1990, A&A, 239, 78
Oliva, E., Moorwood, A. F. M., & Danziger, I. J. 1989, A&A, 214, 307
Panagia, N. 1973, AJ, 78, 929
Piña, R. K., Jones, B., Puetter, R. C., & Stein, W. A. 1992, ApJ, 401, L75
Rotaciuc, V., Krabbe, A., Cameron, M., Drapatz, S., Genzel, R., Sternberg, A., & Storey, J. W. V. 1991, ApJ, 370, L23
Saikia, D. J., Unger, S. W., Pedlar, A., Yates, G. J., Axon, D. J., Wolstencroft, R. D., Taylor, K., & Gyldenkerne, K. 1990, MNRAS, 245, 397
Scoville, N. Z., Soifer, B. T., Neugebauer, G., Young, J. S., Matthews, K., & Yerka, J. 1985, ApJ, 289, 129
Telesco, C. M., & Harper, D. A. 1980, ApJ, 235, 392
Ulvestad, J. S., & Antonucci, R. R. J. 1991, AJ, 102, 875
van der Werf, P., Cameron, M., Genzel, R., Blietz, M., Krabbe, A., Forbes, D. A., & Ward, M. J. 1993, in Astronomy with Millimeter and Submillimeter Wave Interferometry, ed. M. Ishiguro (ASP Conf. Ser.), in press
Waller, W. H., Kleinmann, S. G., & Ricker, G. R. 1988, AJ, 95, 1057
Wright, G. S., & Joseph, R. D. 1989, in Infrared Spectroscopy in Astronomy, ed. B. H. Kaldeich (Nordwijk: ESA), 535